



The effects of the rock bridge ligament angle and the confinement on crack coalescence in rock bridges: An experimental study and discrete element method

Wen Wan^{a,*}, Jie Liu^a, Yanlin Zhao^a, Xiang Fan^b

^a School of Resource, Environment and Safety Engineering, Hunan University of Science and Technology, Xiangtan, China

^b School of Highway, Chang'an University, Xi An, China

ARTICLE INFO

Article history:

Received 23 July 2018

Accepted 6 December 2018

Available online 21 June 2019

Keywords:

Crack coalescence

Stress concentrations

Tensile crack

Shear crack

ABSTRACT

The present article investigates the influences of the rock bridge ligament angle, β , and the confinement on crack coalescence patterns by conducting laboratory and numerical tests on rock-like specimens. Laboratory tests show that no coalescence in the rock bridge occurred for low β . With an increase of β , tensile-shear coalescence and tensile coalescences subsequently occurred. In addition, the increase in the confinement first promoted shear coalescence and then restrained crack coalescence for low β , whereas the tensile coalescence was restrained by the increase in confinement for high β . The numerical results corroborate the laboratory tests in the coalescence patterns. In addition, the numerical study shows that tensile and shear cracks subsequently initiated near crack tips because of the concentrated tensile and shear stresses, respectively. Regarding the influence of β on crack coalescence, tensile or shear stress failed to concentrate in rock bridges for low β . Therefore, the cracks failed to coalesce, whereas with the increase in β , tensile and shear stress concentrations occurred in the bridge and led to either tensile shear or tensile coalescence. Regarding the influence of confinement on crack coalescence, the increase in confinement restrained the tensile stress concentrations and further hindered tensile crack coalescence in rock bridges for high values of β .

© 2019 Académie des sciences. Published by Elsevier Masson SAS. All rights reserved.

1. Introduction

Small fractures, widely existing in rocks, may significantly affect the mechanical properties of rocks because cracks, initiating from these small fractures, may coalesce and then lead to the failure of the rock. Thus, extensive studies have investigated crack development in rocks or rock-like specimens containing small fractures [1–9]. Previous studies indicated that many internal factors (crack sizes, the inclination angle of the crack, the rock bridge angle, etc.) and extensive external factors (loading mode and loading rate) significantly affect crack development. For instance, Haeri et al. showed through laboratory and numerical studies that the length of the crack affects the breakage path of disk specimens that contain one or two prefabricated cracks [10]. Li and Wong proposed that the inclination angle of the prefabricated crack and the distribution of the rock bridge angle influence crack development [11]. The studies by Cao et al. and Zhao et al. showed

* Corresponding author.

E-mail address: wenwanhust@126.com (W. Wan).

Table 1
Main mechanical properties of the rock-like material.

| | Uniaxial compressive strength (MPa) | Elastic modulus (GPa) | Poisson ratio |
|-------|-------------------------------------|-----------------------|---------------|
| Value | 22.8 | 2.3 | 0.24 |

that the inclination angle and the rock bridge ligament angle are two important internal factors affecting crack coalescence [12,13]. In addition, by applying the innovative strain monitor method, Zhao et al. further proposed that wing cracks may coalesce for high rock bridge ligament angles [13]. A numerical study based on the discrete method by Zhou and Yang showed similar results [14]. However, the effect of the inclination angle of prefabricated cracks seems unpredictable. For the influence of external factors on crack propagation, first, the innovative semicircular bend tests by Dai et al. showed that the loading rate affects the flexural tensile strength [15]. Recently, they further stated that the dynamic loading rates significantly affect the positions of the critical fracturing profiles [16]. In addition, Erarslan and Williams stated that extra fatigue cracks form around the prefabricated cracks [17]. Cyclic uniaxial tests, performed instead of the static tests by Liu et al., indicated that the failure mode of the jointed specimen is highly dependent on the cyclic parameters and that the tensile splitting mode dominates [18,19].

With other studies [20–23], previous researchers have proposed seven types of cracks frequently observed in jointed specimens [24]. According to the different initiation sequences, cracks have been classified into wing cracks and secondary cracks. Wing cracks first initiate and frequently propagate along the maximum compression direction. Subsequently, secondary cracks, including shear, tensile or shear-tensile cracks, may propagate in various directions. In addition, by comprehensively analyzing the differences in the initiation sequence, location, and mode, Zhou et al. further proposed five types of cracks [25]. To comprehensively investigate the crack coalescence that occurs between fractures when cracks propagate, convenient numerical and laboratory studies have been conducted instead of the time-consuming field investigations [26–30]. In particular, the numerical simulations based on the discrete element method (DEM) can successfully and rapidly reproduce the fracture of the brittle rock or rock-like specimens because the numerical data, including the forces, bond breakages, and particle displacement, are accessible at any stage of the simulation. Then, we can directly simulate the physical micromechanics [31–33]. However, some limitations to DEM exist. First, the fracture is closely related to the size of the elements (size effect). Second, a cross effect exists because of the difference between the size and shape of elements with real grains. Third, to establish the relationship between the local and macroscopic constitutive laws, data obtained from classical geo-mechanical tests, which may be impractical, are used [34].

The aforementioned studies significantly contributed to understanding the crack initiation sequence and the coalescence patterns for various rock bridge ligament angles. However, the impetus of the crack development remains unclear. Recently, numerical studies of rock-like specimens containing a single prefabricated fracture by Xie and Liu showed that stress concentrations occurred when the specimen was uniaxially compressed; then, cracks initiated when the concentrated stresses were high enough [35,36]. These two studies focused on the stress evolution of a specimen containing one prefabricated fracture. However, in most rock engineering, the rock is in biaxial states characterized by various confinements and numerous small fractures. Thus, crack coalescence in biaxial states deserves further study.

In the present article, first, a series of uniaxial compression tests was conducted to investigate the effect of the rock bridge ligament angle (β) on the crack coalescence in rock bridges. Then, another series of biaxial compression tests were performed to study the influence of the confinement on the crack propagation in rock bridges. More importantly, because of the ability of DEM to directly observe crack propagation [31–33], we further studied the impetus for crack development using Particle Flow Code 2D (PFC 2D).

2. Laboratory tests

2.1. Laboratory test preparation and apparatus

The rock-like specimens, widely used to investigate the characteristics of crack propagation, consisted of cement, sand, and water with a volume ratio of 2:2:1 [5]. The height, width, and thickness of the specimens were 150 mm, 150 mm, and 30 mm, respectively. To create the pre-existing small fractures, two thin mica sheets with a length and a thickness of 20 mm and 0.3 mm, respectively, were inserted into the mortar at specific positions after pouring the blended mortar into the mold. After a curing process of 24 h, the plates were removed, and then the specimens were unmolded and cured for 28 days in water. The main mechanical properties of the intact specimen were obtained by conducting uniaxial compression tests (Table 1).

Fig. 1(a) depicts the geometry of the specimen containing two parallel fractures characterized by the fracture inclination angle, α , and the rock bridge ligament angle, β . The red and green lines denote the two fractures with a length of 2 cm. In the present article, to investigate the influence of β on the crack coalescence under uniaxial compressions, two groups of specimens were tested in Series A (Table 2). In addition, to test the influence of the lateral confinement on the crack coalescence, the lateral confinements (σ_3) were 0 MPa, 0.5 MPa, and 1 MPa in Series B, respectively (Table 2).

The compression tests were conducted on the RLY-600 testing platform (Fig. 2). This platform, consisting of a rigid loading frame and a control system, can provide compression loads in two perpendicular directions. The elastic modulus of

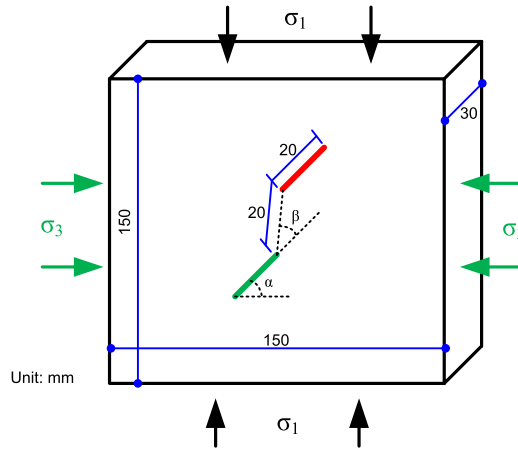


Fig. 1. Specimen geometry: α and β are the fracture inclination angle and the rock bridge ligament angle, respectively.

Table 2
Details of the tests.

| | | β ($^{\circ}$) | | | |
|----------|-------------------------------|------------------------|-----|-----|-----|
| | | 0 | 30 | 60 | 90 |
| Series A | α ($^{\circ}$) | | | | |
| | 30 | S01 | S02 | S03 | S04 |
| | 45 | S05 | S06 | S07 | S08 |
| | | σ_3 (MPa) | | | |
| | | 0 | 0.5 | 1 | - |
| Series B | $\alpha-\beta$ ($^{\circ}$) | | | | |
| | 30-0 | S01 | S09 | S10 | - |
| | 30-30 | S02 | S11 | S12 | |
| | 30-60 | S03 | S13 | S14 | |
| | 30-90 | S04 | S15 | S16 | |
| | 45-0 | S05 | S17 | S18 | - |
| | 45-30 | S06 | S19 | S20 | |
| | 45-60 | S07 | S21 | S22 | |
| | 45-90 | S08 | S23 | S24 | |



Fig. 2. Testing apparatus: (a) loading frame, (b) high-speed camera.

the loading plates was approximately 200 GPa. In compression tests, the axial load (σ_1) was displacement controlled with a constant rate of 0.0005 mm/s. The axial force and the displacement were recorded every few seconds. In addition, the loading process was recorded using a high-resolution camera (Fig. 2).

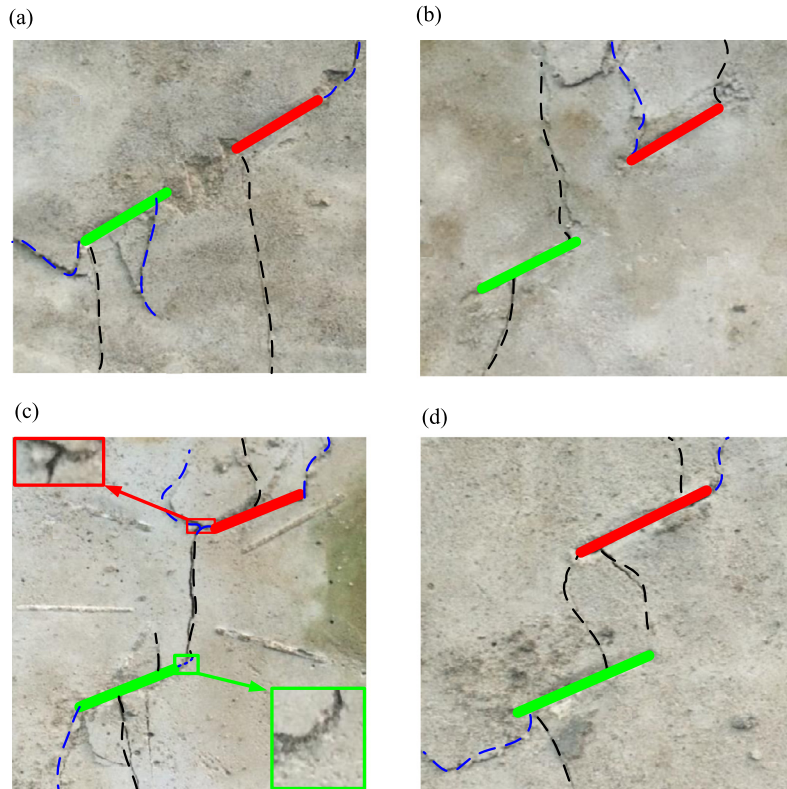


Fig. 3. Crack propagation for various rock bridge ligament angles: (a), (b), (c), and (d) are the crack propagations for S01, S02, S03, and S04, respectively.

2.2. Laboratory results

(1) The effect of β on the crack coalescence

Fig. 3 depicts the typical crack coalescence for $\alpha = 30^\circ$. When $\beta = 0^\circ$, Fig. 3(a) shows that the cracks in the rock bridge failed to coalesce. When β increase up to 30° , Fig. 3(b) shows that three tensile cracks (TC), denoted by the black dash lines, and a shear crack (SC) in blue initiated near the fracture tips. However, the cracks still failed to coalesce in the rock bridge. With a further increase in β up to 60° , the cracks in the rock bridges coalesced (Fig. 3(c)). The magnified cracks in the red and green rectangles show that this coalescence crack may have partly resulted from shear force, because shear cracks are frequently characterized by their relatively large thickness and abrasion [36]. The uneven part, in the black dash line, shows that this coalescence may also result from tensile crack propagation [36]. In addition, several tensile and shear cracks, shown in red and blue dashed lines, also formed. When $\beta = 90^\circ$, Fig. 3(d) indicates that a tensile crack coalesced in the rock bridge, and another tensile crack approximately coalesced. This coalescence pattern has also been observed in previous studies [10].

The above descriptions show that the rock bridge coalescence pattern varied from no coalescence (NC) to tensile-shear coalescence (T-SC) to tensile coalescence (TC) as β increased. Similar phenomena were also observed for $\alpha = 45^\circ$ (Fig. 4). The above variation in coalescence agrees well with previous results [12,13]. Thus, we can conclude that tensile coalescence is favorable for high β . However, the impetus for this phenomenon, which remains unknown, will be discussed in the following numerical study.

(2) The effect of confinement on crack coalescence

Figs. 5 and 6 show typical crack coalescences under various confinements for low and high values of β . First, for low β , when the confinement was 0 MPa, cracks failed to coalesce (NC) in the rock bridge (Figs. 5(a1) and (a2)). However, shear cracks coalesced (SC) when the confinement increased to 0.5 MPa (Figs. 5(b1) and (b2)). With further increase in confinement, the rock bridge remained intact (NC). In addition, the tensile crack colored in black shows that the increase in confinement restrained tensile crack propagation. A similar phenomenon was observed for $\alpha = 45^\circ$ (Table 3).

For high rock bridge angles of 90° , when confinement was 0 MPa, a tensile crack connected two crack tips from the upper and bottom cracks, and another tensile crack approximately coalesced (TC) in the rock bridge (Fig. 6(a)). However, when the confinement increased to 0.5 MPa (Fig. 6(b)), only one tensile crack formed in the rock bridge (TC). With a further

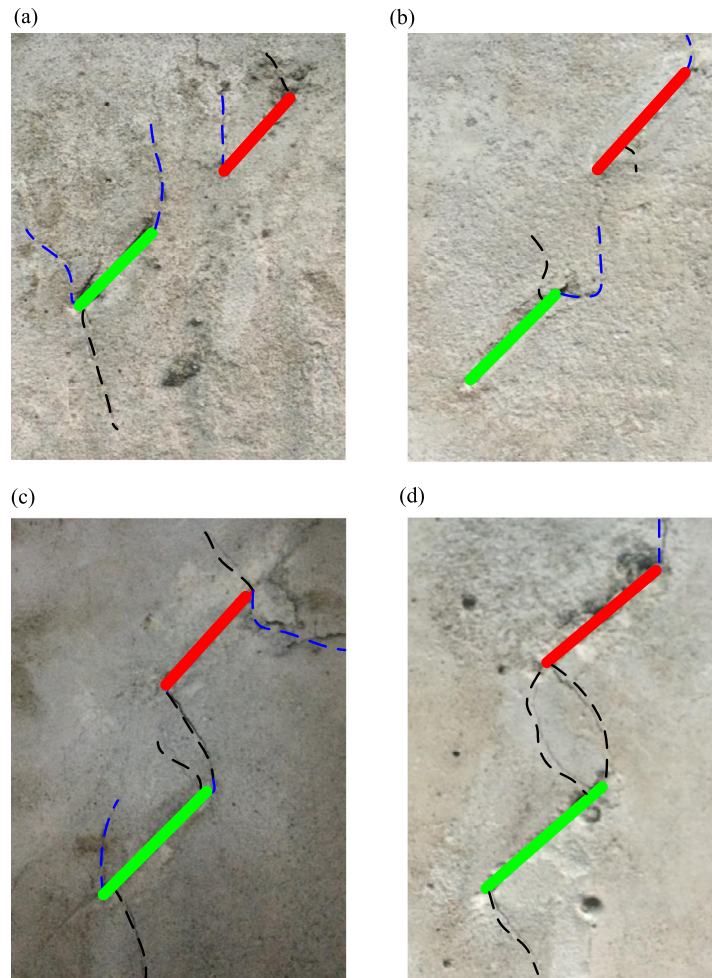


Fig. 4. Crack propagation for various rock bridge ligament angles: (a), (b), (c) and (d) are the crack propagation for S05, S06, S07, and S08, respectively.

increase in confinement, a tensile crack initiated from the bottom crack; however, it failed to connect to the tip of the upper crack (NC). With the crack coalesce patterns for the inclination and rock bridge angles of 45° and 90° in Table 3, we can infer that the increase in confinement restrains tensile crack propagation and tensile coalescence for high β . However, because of the limit in laboratory tests to dynamically monitor the stress distributions in the loading process, the impetus of crack propagation remains unclear and deserves further numerical investigation.

3. Numerical tests

3.1. Numerical model and specifications

Particle Flow Code 2D is a universal discrete element method program, used to simulate rock behaviors, especially rock fracture characteristics [31–33]. In PFC 2D, a numerical model consists of three elements, namely, particles, bonds, and walls. In the present article, because the parallel bonds can more accurately simulate the contact between the grains in rock [5,32], the model consisted of 54,323 particles and 16,339 parallel bonds (Fig. 7). The micro and macro properties of the model are listed in Table 4. The stiffness of the boundary walls was 200 GPa, which was in accordance with the laboratory loading plates. Before calculations, we conducted a calibration on the uniaxial compressive strength and the elastic modulus to make the numerical results comparable [1,5]. The geometry, uniaxial compression strength, and elastic modulus were close to the laboratory values. Therefore, the model is reasonable. To simulate the axial load, the bottom wall was fixed, and the upper wall was controlled with a constant rate. In addition, the lateral walls were servo-controlled to provide constant confinement in the loading process. Moreover, 5625 measurement circles were installed to dynamically monitor the tensile and shear stresses that are responsible for crack propagation in the compression process. Every measurement circle included more than six particles (Fig. 7); therefore, the average stresses, including the shear stress, τ , the horizontal stress, σ_h , and

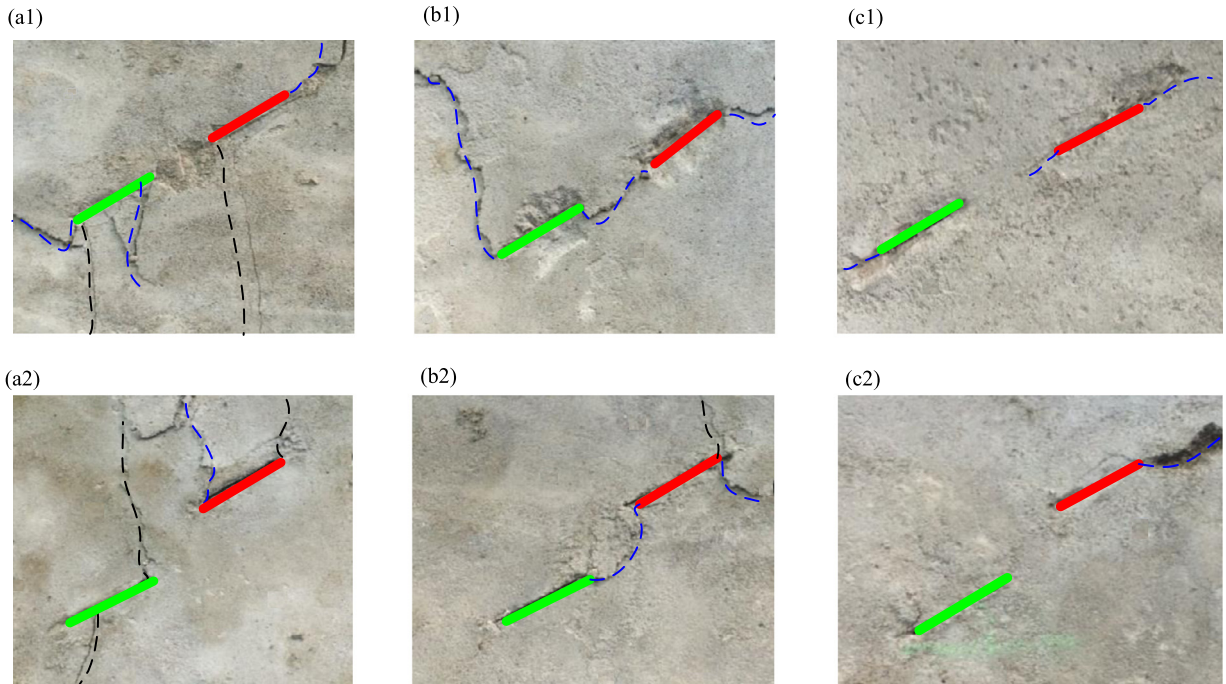


Fig. 5. Crack coalescences for various confinements: (a1), (b1), and (c1) are the coalescence of specimens S01, S09, and S10, respectively; (a2), (b2), and (c2) are the coalescence of specimens S02, S11, and S12, respectively.

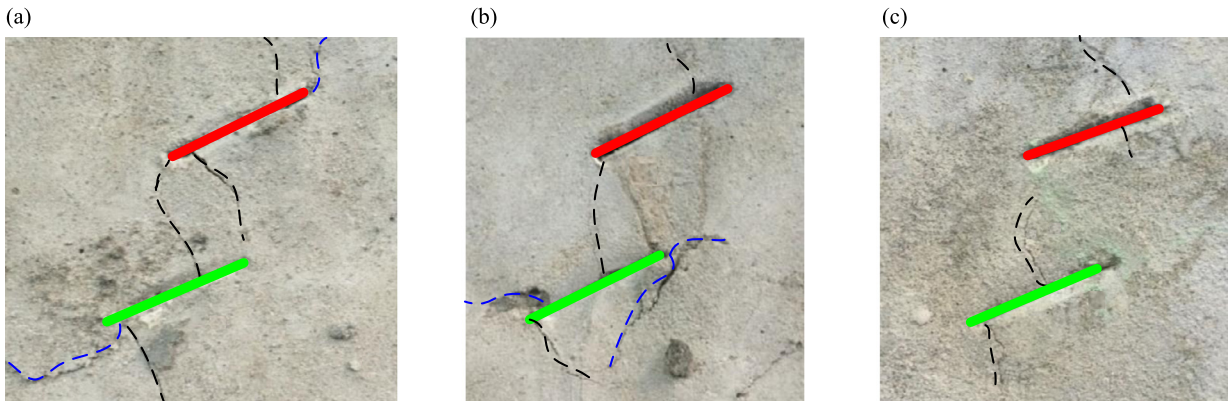


Fig. 6. Crack coalescences for various confinements: (a), (b), and (c) are the coalescence conditions of specimens S04, S15, and S16, respectively.

Table 3
Crack types for coalescence in rock bridges.

| Series B | $\alpha-\beta$ (°) | σ_3 (MPa) | | |
|----------|--------------------|------------------|------|----|
| | | 0 | 0.5 | 1 |
| | 30–0 | NC | SC | NC |
| | 30–30 | NC | SC | NC |
| | 30–60 | T-SC | SC | NC |
| | 30–90 | TC | TC | NC |
| | 45–0 | NC | SC | NC |
| | 45–30 | NC | SC | NC |
| | 45–60 | T-SC | NC | NC |
| | 45–90 | TC | T-SC | NC |

the vertical stress, σ_v , can represent the stress conditions at this point. Then, because the compressive stress in PFC 2D is negative, the maximum principle stress (tensile stress) can be written as:

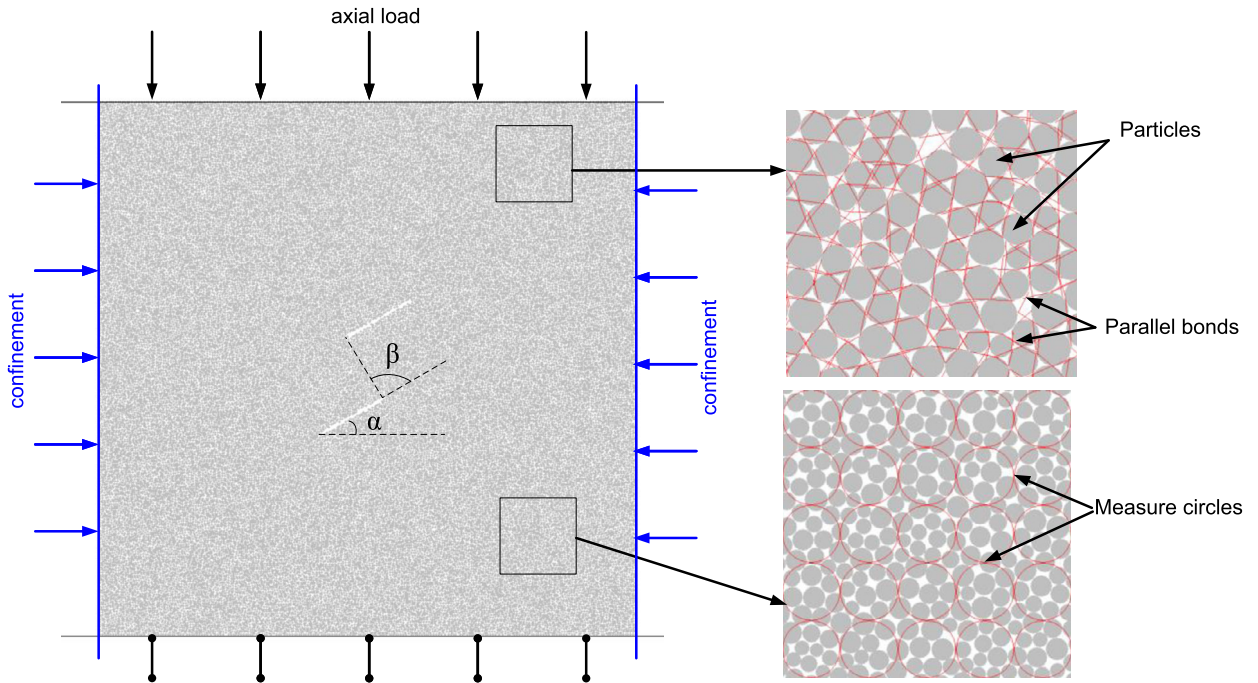


Fig. 7. Numerical model.

Table 4
Micro and macro properties of the numerical model.

| Micro-parameters | Values | Macro parameters | Value |
|--|--------|--|-------|
| Minimum radius (mm) | 0.24 | Uniaxial compression stress, UCS (MPa) | 22.3 |
| Rmax/Rmin | 1.66 | Young's modulus, E (GPa) | 2.1 |
| Particle density (kg/m^3) | 2050 | | |
| Particle contact modulus (GPa) | 9.5 | Poisson ratio 0.24 | |
| The ratio of the normal stiffness to shear stiffness of particles | 2.5 | | |
| Friction coefficient | 0.5 | | |
| Parallel bond modulus (GPa) | 1.95 | | |
| The ratio of the normal stiffness to shear stiffness of parallel bonds | 2.5 | | |
| Parallel bond normal strength (MPa) | 15.7 | | |
| Parallel bond shear strength (MPa) | 15.7 | | |
| Boundary stiffness (GPa) | 200 | | |

$$\sigma_{\max} = \frac{\sigma_h + \sigma_v}{2} + \sqrt{\left(\frac{\sigma_h - \sigma_v}{2}\right)^2 + \tau^2}$$

3.2. Stress evolutions for various rock bridge angles

Fig. 8 depicts the typical axial stress–strain curves for specimens S01, S02, S03, and S04. Clearly, the numerical data slightly deviate from the laboratory data. In addition, a similar phenomenon was observed for the other specimens (figures not shown). Thus, these numerical simulations are feasible.

To investigate the stress distributions that might be responsible for crack propagation, the tensile and shear stresses for various β were recorded. When the axial strain was 2.1% for α and β of 30° and 0° , respectively, the stress distribution in Fig. 9(a1) shows that four tensile stress concentration zones (T1–T4) formed near the fracture tips before tensile crack initiation. Simultaneously, shear stress concentrations also formed at the fracture tips (Fig. 9(b1)). In addition, the tensile stress zones failed to overlap in the rock bridge. In other words, the rock bridge was dominated by the compression stress instead of the tensile stress.

When the axial strain increased to 4.0%, four tensile cracks (TC1–TC4) formed (Fig. 9(a2)). Clearly, the initiation points of these cracks overlapped with the tensile stress concentration points in Fig. 9(a1). In addition, Fig. 9(a2) shows that the

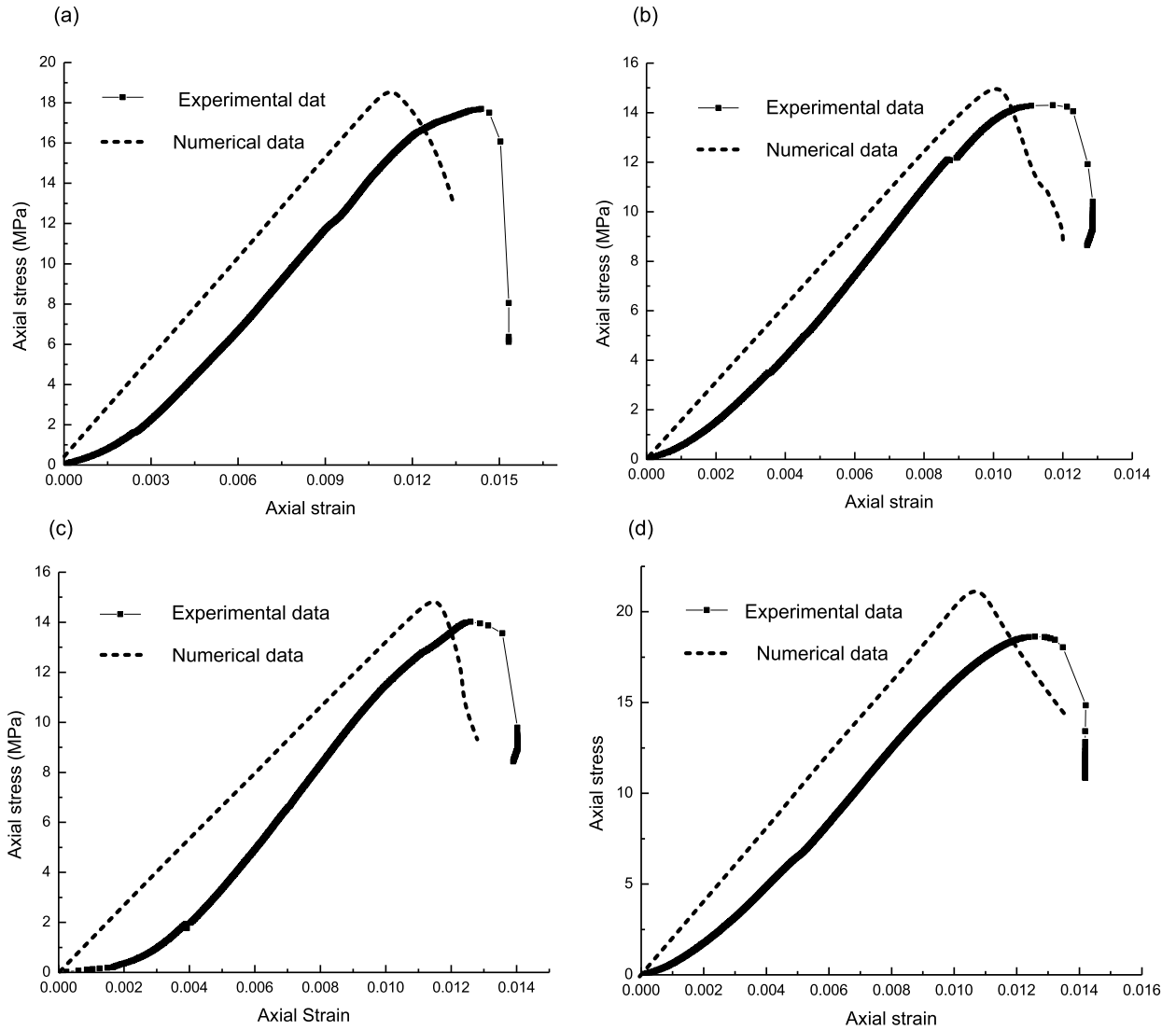


Fig. 8. Typical axial stress-strain curves for laboratory and numerical tests: (a), (b), (c), and (d) are the curves for specimens S01, S02, S03, and S04.

tensile stresses still concentrated at these crack tips. However, these concentrations slightly dissipated. Moreover, Fig. 9(b2) shows that shear stress concentrations were promoted, and six shear planes (SP1–SP6) formed ahead of the fracture tips.

When the axial strain further increased to 4.9%, the tensile cracks ceased to propagate, and the tensile stress concentrations at these crack tips further dissipated (Fig. 9(a3)). Simultaneously, a crack (SC1) initiated from the right tip of the upper fracture (Fig. 9(a3)). This crack, overlapping with the SP1, consisted of the red and the black micro cracks. Therefore, according to previous studies [13,36], this crack is a shear crack. The stress distribution in Fig. 9(b3) shows that shear stress was further concentrated, especially on SP2, SP3, and SP6. These promoted concentrations were responsible for shear crack propagation in Fig. 9(a4). The crack distribution in Fig. 9(a4) shows that cracks failed to coalesce in the rock bridge for the low crack inclination angle. This result agrees well with the laboratory results in Fig. 9(b4). We can conclude from the above descriptions that tensile and shear cracks subsequently initiate near the fracture tips, because of the tensile and shear stress concentrations. In addition, for the tensile cracks, tensile stress concentrations dissipated when the crack propagated. When the tensile stress is lower than a critical value, the tensile crack ceases to propagate.

When β increased to 60° , Fig. 10(a1) shows that four tensile stress concentration zones formed near the fracture tips before tensile crack propagation. In addition, the shear and the tensile concentration zones of the upper and the bottom cracks overlapped. When the axial strain increased to 3.9%, Fig. 10(a2) shows that four tensile cracks formed because of the concentrated tensile stresses (T1–T4 in Fig. 10(a1)). The stress concentrations in Fig. 10(a2) show that the tensile stresses at the crack tips dissipated slightly. It is interesting to note that the fifth tensile concentration zone (T5) formed at the middle of the rock bridge and led to the formation of TC5 in Fig. 10(a2). In addition, four shear planes (SP1–SP4) formed. Then, TC5 propagated (Fig. 10(a3)) and led to the dissipation of the tensile stress at the rock bridge. Similar crack propagation

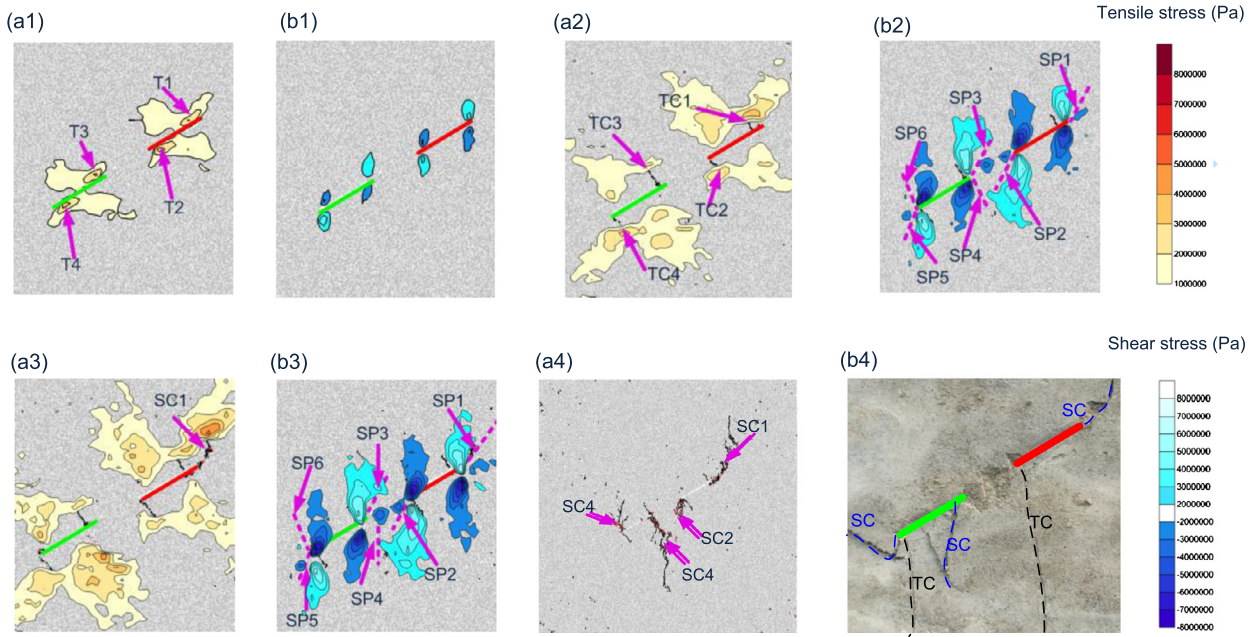


Fig. 9. Crack propagations and stress distributions for S01: (a1)–(a3) are the tensile stress concentrations for axial strains of 2.1%, 4.0% and 4.9%, respectively; (b1)–(b3) are the corresponding stress distributions at these strains, respectively; (a4) and (b4) are the numerical and laboratory crack propagation, respectively.

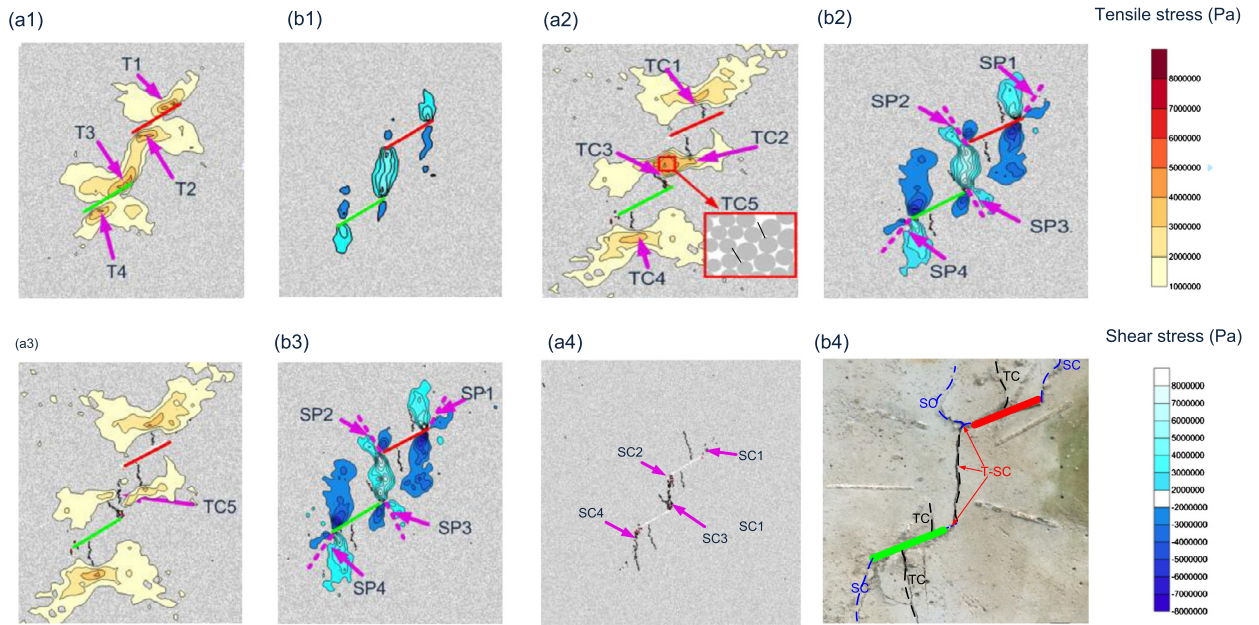


Fig. 10. Crack propagations and stress distributions for S03: (a1)–(a3) are the tensile stress concentrations for axial strains of 2.5%, 3.9%, and 5.3%, respectively; (b1)–(b3) are the corresponding shear stress distributions at these strains, respectively; and (a4) and (b4) are the numerical and laboratory crack propagations, respectively.

was reported by Zhang and Wong [37]. Simultaneously, shear stress concentrations continued and led to the formation of SC1–SC4. SC2 and SC3 connected with the tensile crack (TC5) in the rock bridge. The above description shows similar results for a β of 0° where tensile and shear crack subsequently initiated because of the concentrated stresses. However, the increase in β led to tensile and shear stress concentrations in the rock bridge, and further caused crack coalescence.

When β further increased to 90° , similar tensile stress concentrations and overlaps were observed before crack propagation (Figs. 11(a1) and 11(b1)). With further increase in the axial strain, TC1, TC2, and TC4 formed because of the concentrated tensile stresses. However, the tensile stress at crack TC3 further increased (Fig. 11(a2)). The tensile stress

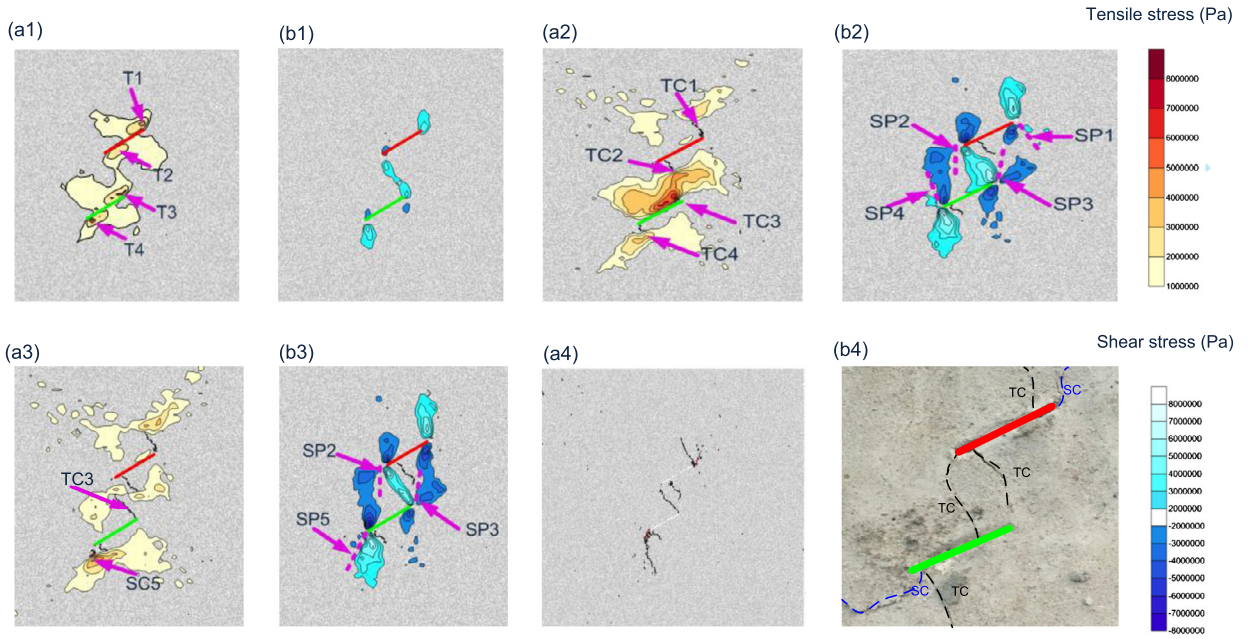


Fig. 11. Crack propagations and stress distributions for S04 (a1)–(a3) are the tensile stress concentrations for the axial strain of 3.9%, 4.1%, and 4.3%, respectively; (b1)–(b3) are the corresponding shear stress distributions at these strains, respectively; (a4) and (b4) are the numerical and laboratory crack propagations, respectively.

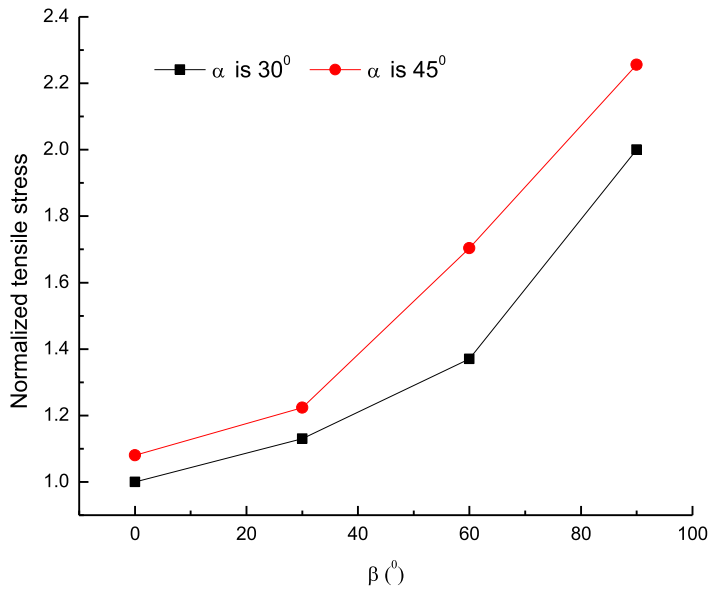


Fig. 12. The maximum values of the normalized tensile stress in rock bridges.

zone approximately covered the entire rock bridge. In addition, four shear planes formed ahead of the fracture tips. Then, the concentrated tensile stress led to the propagation of TC3 (Fig. 11(a3)). The propagation of the tensile crack led to the dissipations of tensile stresses at the crack tips, and the coalescence in the rock bridge (Fig. 11(b4)). Subsequently, shear cracks formed because of the concentrated shear stresses.

The above descriptions indicate that tensile cracks first initiated near crack tips because of the concentrated tensile stresses. Subsequently, the shear concentrations on the shear plane led to shear crack formation. In addition, the maximum values of the normalized tensile stress in Fig. 12 show that the increase in β promoted the tensile stress concentrations in the rock bridge. Therefore, tensile coalescence is favorable at high values of β . This numerical conclusion can properly verify the laboratory and numerical phenomena.

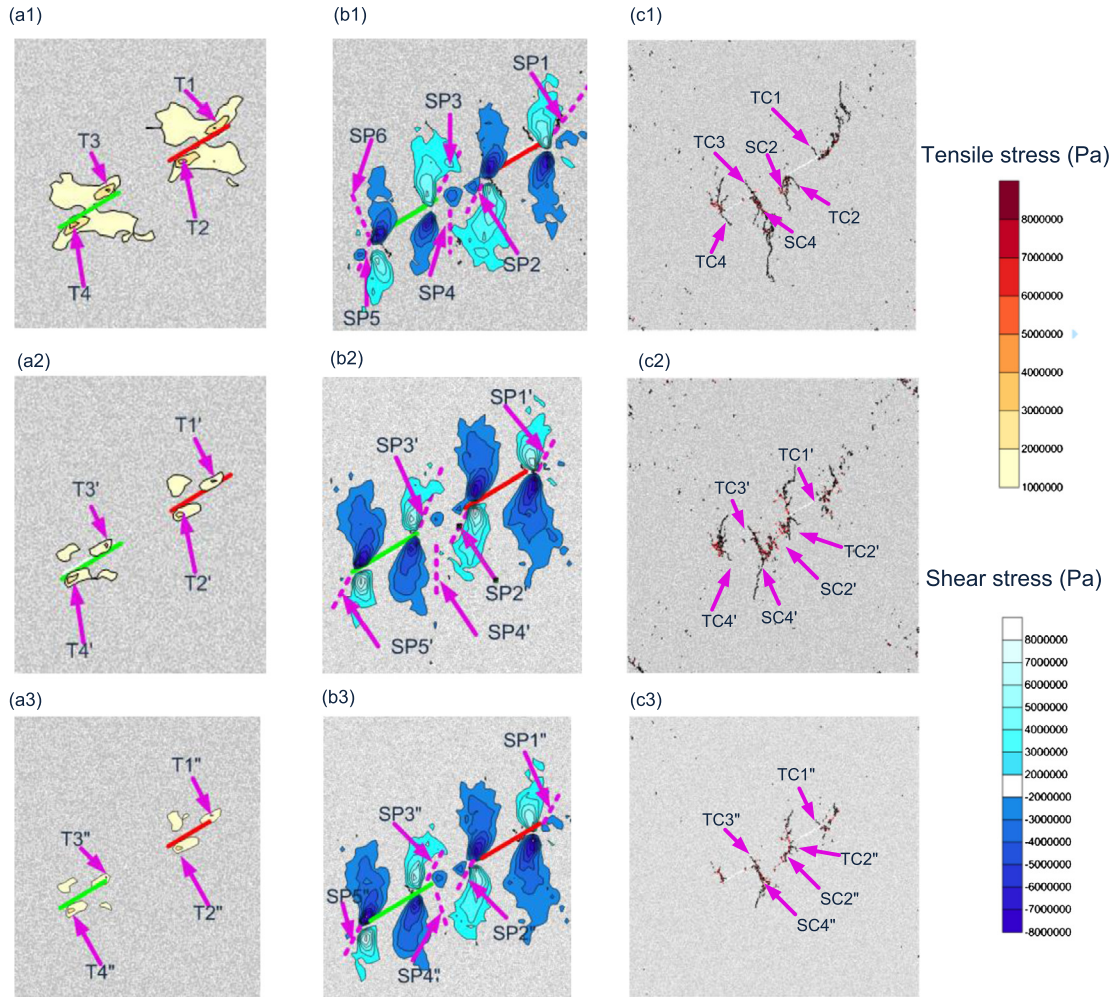


Fig. 13. Stress concentrations and crack propagation for various confinements: (a1), (a2) and (a3) are the tensile stress concentration before tensile crack initiation when the confining stresses are 0 MPa, 0.5 MPa, and 1 MPa, respectively; (b1), (b2), and (b3) are the corresponding shear stress concentrations before shear crack propagations in the rock bridge for this pressure, respectively; and (c1), (c2), and (c3) are the crack distributions when the axial strain is 5.1% at these pressures, respectively.

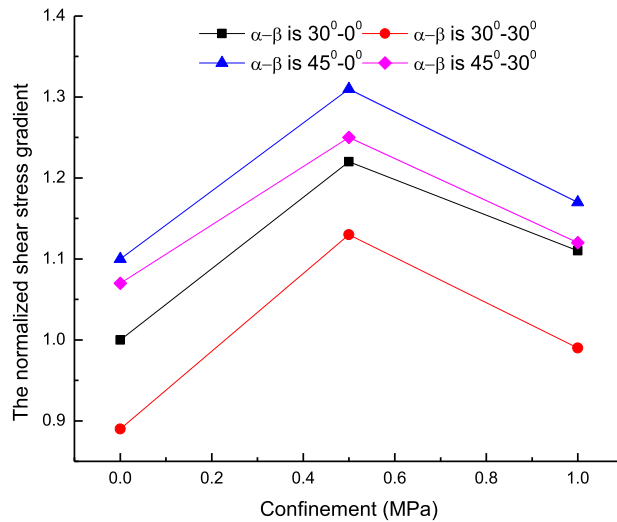


Fig. 14. The normalized shear stress gradient in the rock bridge before shear crack propagation.

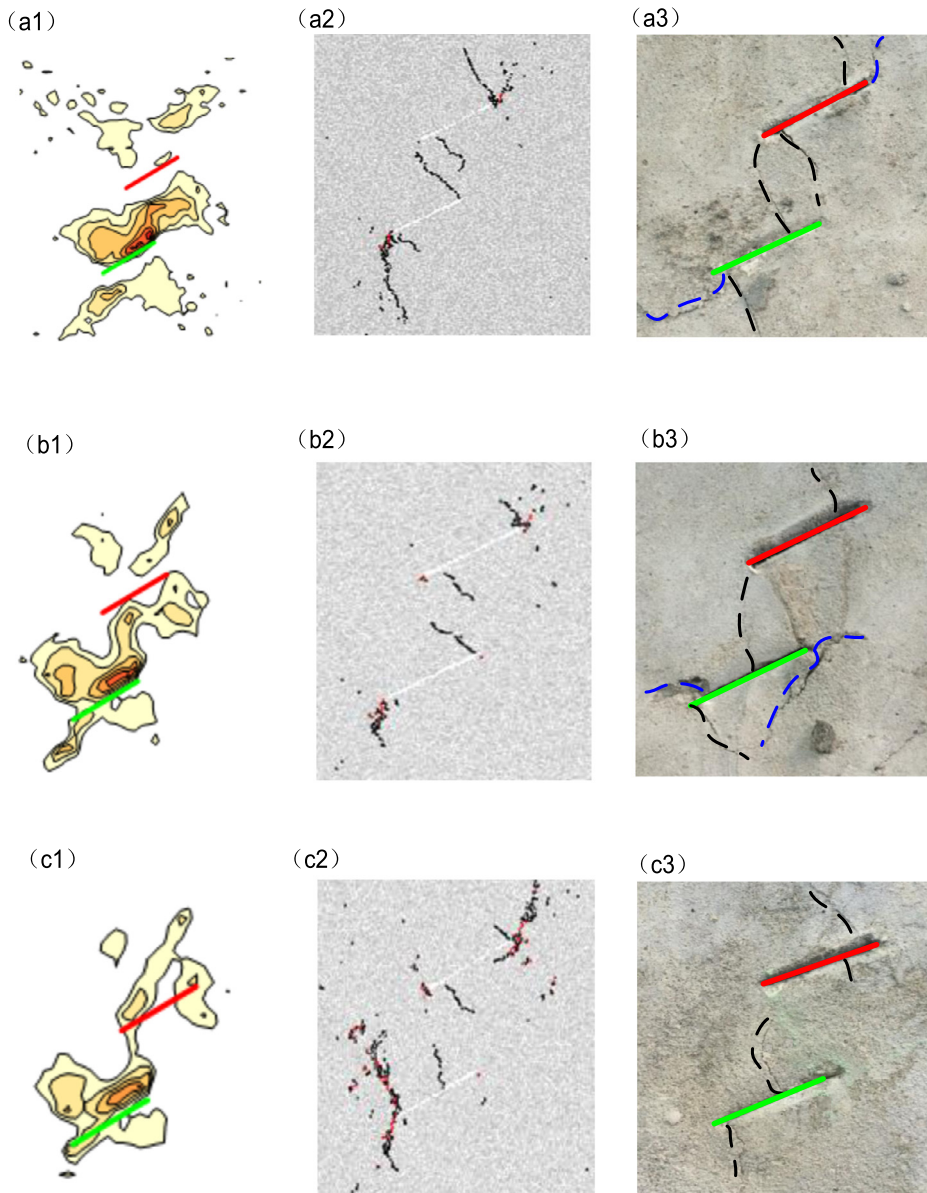


Fig. 15. Influence of confinements on crack coalescence when α and β are 30° and 90° , respectively: (a1), (b1), and (c1) are the tensile stress distributions when the maximum tensile stress occurred in rock bridges for confinements of 0 MPa, 0.5 MPa, and 1 MPa, respectively; (a2), (b2), and (c2) are the numerical crack propagation of these pressures, respectively; and (a3), (b3), and (c3) are the laboratory crack propagation of these pressures, respectively.

3.3. Stress evolutions in rock bridges for various confinements

The above laboratory tests show that the increase in confinement may first promote, and then restrain shear crack coalescence for low β in the rock bridge. Fig. 12 shows the typical stress conditions and crack propagation for various confinements when α and β are 30° and 0° , respectively. Clearly, the increase in confinement restrained the tensile stress concentrations before tensile crack propagation (Figs. 13(a1)–(a3)). Correspondingly, the lengths of the tensile (wing) cracks gradually decreased (Figs. 13(c1)–(c3)). Before shear crack propagation in the rock bridge, a shear plane (SP2) with a shear stress gradient of approximately 9 MPa formed (Fig. 13(b1)). When the confinement increased to 0.5 MPa, a similar shear plane (SP2') formed. However, the shear stress gradient increased to approximately 11 MPa (Fig. 13(b1)). This increased shear stress gradient may promote the propagation of SC2' and further promote shear crack coalescence in the rock bridge (Fig. 13(c2)). With further increase in the confinement, the shear stress gradient decreased to approximately 10 MPa; thus, the shear crack, SC2'', failed to coalesce in the rock bridge (Fig. 13(c3)). The numerical results agree well with the laboratory tests (Figs. 5(a1)–(c1)). The normalized shear stress gradients before shear crack propagation in the rock bridge show similar results for low β (Fig. 14). Thus, we can conclude that, for low β , the increase in confinement restrains tensile crack

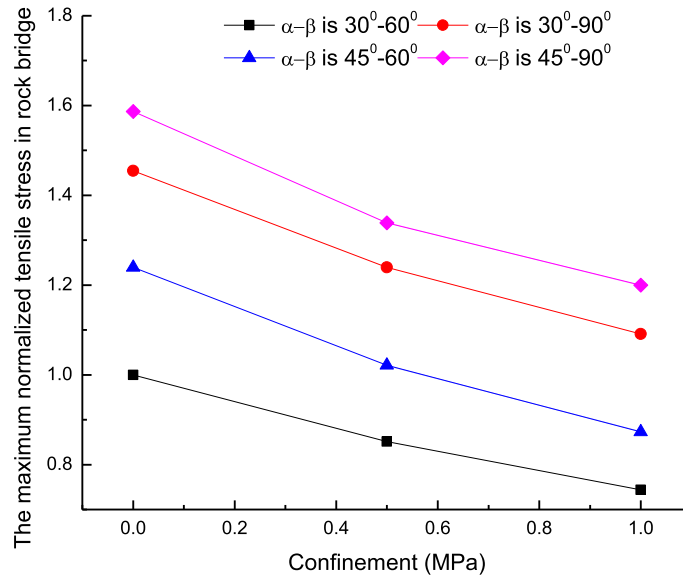


Fig. 16. Maximum tensile stresses in rock bridges for various confinements.

propagation. In addition, this increase first promotes shear concentration, and then restrains shear concentration in the rock bridge.

The numerical results indicate that the highly concentrated tensile stress is responsible for the tensile crack coalescence in rock bridges. Therefore, in the following part, we mainly focus on the tensile stress distributions in rock bridges for high β . When the confinement is 0 MPa, a highly concentrated tensile zone forms in the rock bridge. This zone is responsible for the tensile coalescence in rock bridges (Figs. 15(a2) and (a3)). When the confinement increased to 0.5 MPa, the area of the tensile zone and the maximum tensile stress in the rock bridge decreased (Fig. 15(c1)). Therefore, the tensile crack propagations in Figs. 15(b2) and (b3) were restrained. With further increase in confinement, tensile concentration and tensile crack propagation in rock bridges are further restrained. Thus, we may infer that the increase in confinement may restrain tensile stress concentration in the rock bridge for high β . The normalized value of the maximum tensile stress in Fig. 16 can properly verify this inference. Thus, the increase in confinement will restrain the tensile coalescence in rock bridges.

4. Conclusions

To investigate the influences of β and the confinement on crack coalescence in rock bridges, we performed laboratory and numerical tests. The results show that the concentrated tensile and shear stresses are responsible for crack propagation in the rock bridge. First, the increase in β promotes the tensile concentration in the rock bridge; thus, tensile crack coalescences in rock bridges are favorable for high β . Second, the increase in confinement restrains tensile stress concentrations and then further hinders tensile crack coalescence. In addition, for low values of β , we interestingly found that the increase in confinement first promotes shear crack coalescence in rock bridges and subsequently restrains crack coalescence.

Acknowledgements

The authors would like to acknowledge these financial supports: Projects (51804110, 51774131, 51774132) supported by the National Natural Science Foundation of China and the China Postdoctoral Science Foundation (2017M612557).

References

- [1] J. Jin, P. Cao, Y. Chen, C.Z. Pu, D.W. Mao, X. Fan, Influence of single flaw on the failure process and energy mechanics of rock-like material, *Comput. Geotech.* 86 (2017) 150–162.
- [2] Y.L. Zhao, Y.X. Wang, W.J. Wang, L.M. Tang, Q. Liu, G. Cheng, Modeling of rheological fracture behavior of rock cracks subjected to hydraulic pressure and far field stresses, *Theor. Appl. Fract. Mech.* 101 (2019) 59–66.
- [3] P. Feng, F. Dai, Y. Liu, N.W. Xu, T. Zhao, Effects of strain rate on the mechanical and fracturing behaviors of rock-like specimens containing two unparallel fissures under uniaxial compression, *Soil Dyn. Earthq. Eng.* 110 (2018) 195–211.
- [4] Q.B. Lin, P. Cao, R.H. Cao, Experimental investigation of jointed rock breaking under a disc cutter with different confining stresses, *C. R. Mecanique* 346 (9) (2018) 833–843.
- [5] R.H. Cao, P. Cao, X. Fan, X.G. Xiong, H. Lin, An experimental and numerical study on mechanical behavior of ubiquitous-joint brittle rock-like specimens under uniaxial compression, *Rock Mech. Rock Eng.* 49 (11) (2016) 4319–4338.

- [6] H. Lin, W. Xiong, Q. Yan, Three dimensional effect of tensile strength in the standard Brazilian test considering contact length, *Geotech. Test. J.* 39 (1) (2015) 137–143.
- [7] Y.L. Zhao, L.Y. Zhang, W.J. Wang, W. Wan, W.H. Ma, Separation of elasto visco plastic strains of rock and a nonlinear creep model, *Int. J. Geomech.* (2018), [https://doi.org/10.1061/\(ASCE\)GM.1943-5622.0001033](https://doi.org/10.1061/(ASCE)GM.1943-5622.0001033).
- [8] J. Liu, J. Wang, The effect of indentation sequence on rock breakages: a study based on laboratory and numerical tests, *C. R. Mecanique* 346 (1) (2018) 26–38.
- [9] X. Fan, K.H. Li, H.P. Lai, Y.L. Xie, R.H. Cao, J. Zheng, Internal stress distribution and cracking around flaws and openings of rock block under uniaxial compression: a particle mechanics approach, *Comput. Geotech.* 102 (2018) 28–38.
- [10] H. Haeri, K. Shahriar, M.F. Marji, P. Moarefvand, Experimental and numerical study of crack propagation and coalescence in pre-cracked rock-like disks, *Int. J. Rock Mech. Min. Sci.* 67 (2014) 20–28.
- [11] H.Q. Li, L.N.Y. Wong, Numerical study on coalescence of pre-existing flaw pairs in rock-like material, *Rock Mech. Rock Eng.* 47 (6) (2013) 2087–2105.
- [12] P. Cao, T.Y. Liu, C.Z. Pu, H. Lin, Crack propagation and coalescence of brittle rock-like specimens with pre-existing cracks in compression, *Eng. Geol.* 187 (2015) 113–121.
- [13] Y.L. Zhao, L.Y. Zhang, W.J. Wang, C.Z. Pu, W. Wan, J.Z. Tang, Cracking and stress-strain behavior of rock-like material containing two flaws under uniaxial compression, *Rock Mech. Rock Eng.* 49 (7) (2016) 2665–2687.
- [14] X.P. Zhou, H.Q. Yang, Multiscale numerical modeling of propagation and coalescence of multiple cracks in rock masses, *Int. J. Rock Mech. Min. Sci.* 55 (2012) 15–27.
- [15] F. Dai, K. Xia, J.P. Zuo, R. Zhang, N.W. Xu, Static and dynamic flexural strength anisotropy of Barre granite, *Rock Mech. Rock Eng.* 46 (6) (2013) 1589–1602.
- [16] F. Dai, Y. Xu, T. Zhao, N.W. Xu, Y. Liu, Loading-rate-dependent progressive fracturing of cracked chevron-notched Brazilian disc specimens in split Hopkinson pressure bar tests, *Int. J. Rock Mech. Min. Sci.* 88 (2016) 49–60.
- [17] N. Erarslan, D.J. Williams, Mixed-mode fracturing of rocks under static and cyclic loading, *Rock Mech. Rock Eng.* 46 (5) (2012) 1035–1052.
- [18] Y. Liu, F. Dai, L. Dong, N.W. Xu, P. Feng, Experimental investigation on the fatigue mechanical properties of intermittently jointed rock models under cyclic uniaxial compression with different loading parameters, *Rock Mech. Rock Eng.* 51 (1) (2018) 47–68.
- [19] Y. Liu, F. Dai, P. Feng, N.W. Xu, Mechanical behavior of intermittent jointed rocks under random cyclic compression with different loading parameters, *Soil Dyn. Earthq. Eng.* 113 (2018) 12–24.
- [20] N.A. Al-Shayea, Crack propagation trajectories for rocks under mixed mode I–II fracture, *Eng. Geol.* 81 (1) (2005) 84–97.
- [21] D. Huang, D. Gu, C. Yang, R. Huang, G. Fu, Investigation on mechanical behaviors of sandstone with two preexisting flaws under triaxial compression, *Rock Mech. Rock Eng.* 49 (2) (2015) 375–399.
- [22] M. Jiang, H. Chen, G.B. Crosta, Numerical modeling of rock mechanical behavior and fracture propagation by a new bond contact model, *Int. J. Rock Mech. Min. Sci.* 78 (2015) 175–189.
- [23] Y. Li, J. Peng, F. Zhang, Z. Qiu, Cracking behavior and mechanism of sandstone containing a pre-cut hole under combined static and dynamic loading, *Eng. Geol.* 213 (2016) 64–73.
- [24] L.N.Y. Wong, H.H. Einstein, Systematic evaluation of cracking behavior in specimens containing single flaws under uniaxial compression, *Int. J. Rock Mech. Min. Sci.* 46 (2) (2009) 239–249.
- [25] X.P. Zhou, H. Cheng, Y.F. Feng, An experimental study of crack coalescence behaviour in rock-like materials containing multiple flaws under uniaxial compression, *Rock Mech. Rock Eng.* 47 (6) (2013) 961–1986.
- [26] X.P. Zhang, Q.S. Liu, S.C. Wu, X.H. Tang, Crack coalescence between two non-parallel flaws in rock-like material under uniaxial compression, *Eng. Geol.* 199 (2015) 74–90.
- [27] G. da Silva, H.H.B. Einstein, Modeling of crack initiation, propagation and coalescence in rocks, *Int. J. Fract.* 182 (2013) 167–186.
- [28] S.Y. Wang, S.W. Sloan, D.C. Sheng, C.A. Tang, 3D numerical analysis of crack propagation of heterogeneous notched rock under uniaxial tension, *Tectonophysics* 677–678 (2016) 45–67.
- [29] S.Y. Wang, S.W. Sloan, D.C. Sheng, C.A. Tang, Numerical study of failure behaviour of pre-cracked rock specimens under conventional triaxial compression, *Int. J. Solids Struct.* 51 (5) (2014) 1132–1148.
- [30] R.H.C. Wong, P. Lin, Numerical study of stress distribution and crack coalescence mechanisms of a solid containing multiple holes, *Int. J. Rock Mech. Min. Sci.* 79 (2015) 41–54.
- [31] Y. Liu, F. Dai, T. Zhao, N.W. Xu, Numerical investigation of the dynamic properties of intermittent jointed rock models subjected to cyclic uniaxial compression, *Rock Mech. Rock Eng.* 50 (2017) 89–112.
- [32] D.O. Potyondy, P.A. Cundall, A bonded-particle model for rock, *Int. J. Rock Mech. Min. Sci.* 41 (2004) 1329–1364.
- [33] Y. Xu, F. Dai, N.W. Xu, T. Zhao, Numerical investigation of dynamic rock fracture toughness determination using a semi-circular bend specimen in split Hopkinson pressure bar testing, *Rock Mech. Rock Eng.* 49 (3) (2016) 731–745.
- [34] F.V. Donze, V. Richefeu, S.A. Magnier, Advances in discrete element method applied to soil rock and concrete mechanics, *Electron. J. Geolog. Eng.* 8 (2009) 1–44.
- [35] Y.S. Xie, P. Cao, J. Liu, L.W. Dong, Influence of crack surface friction on crack initiation and propagation: a numerical investigation based on extended finite element method, *Comput. Geotech.* 74 (2016) 1–14.
- [36] J. Liu, J. Wang, Stress evolution of rock-like specimens containing a single fracture under uniaxial loading: a numerical study based on particle flow code, *Geotech. Geolog. Eng.* 38 (1) (2018) 567–580.
- [37] X.P. Zhang, L.N.Y. Wong, Crack initiation, propagation and coalescence in rock-like material containing two flaws: a numerical study based on bonded-particle model approach, *Rock Mech. Rock Eng.* 46 (5) (2012) 1001–1021.